Biomass char gasification by H2O, CO2 and their mixture: Evolution of chemical, textural and structural properties of the chars

Chamseddine Guizani, Mejdi Jeguirim, Roger Gadiou, Francisco Javier Escudero Sanz, Sylvain Salvador

Biomass char gasification by H_2O, CO_2 and their mixture: Evolution of chemical, textural and structural properties of the chars

Chamseddine Guizani [a], Mejdi Jeguirim [b,*], Roger Gadiou [b], Fransisco Javier Escudero Sanz [a], Sylvain Salvador [a]

[a] RAPSODEE, École des Mines d'Albi, Route de Teillet, 81013 Albi CT Cedex 09, France
[b] Institut de Sciences des Matériaux de Mulhouse – IS2M CNRS UMR7361, 15 rue Jean Starcky, 68057 Mulhouse, France

Keywords:
Char gasification
Char structure
Char surface functional groups
Char texture
Mineral species behaviour

A B S T R A C T

The present study aims to understand the phenomenology of char gasification by monitoring the chemical, structural and textural char characteristics through the gasification reaction. Chars from beech wood were gasified under 20%H_2O, 20%CO_2 and 20%H_2O + 20%CO_2 in N_2 at 900° C. The gasification reactions were stopped at 20%, 50% and 70% of char conversion. The char properties were analysed by different analytical techniques such as temperature programmed desorption coupled to mass spectrometry, Raman spectroscopy, Scanning Electron Microscopy, N_2 manometry and X-ray Fluorescence. These analyses provide valuable information on the unfolding of the gasification reactions with H_2O, CO_2 and their mixtures. In particular, it is noted that H_2O and CO_2 gasification reactions follow different pathways. Moreover, during mixed atmosphere, despite that the char reactivity can be fairly expressed by summing the two individual reactivities, this apparent additivity appears to be the result of several competitions and synergies between H_2O and CO_2 reactions.

1. Introduction

Fossil fuel depletion, climate change as well as environmental and human health problems are urging humanity to reconsider its relationship toward natural resources, change its energy policy and adopt a more sober way of living. Biomass as a renewable energies is undoubtedly part of the solution, at least to cope with fossil fuel depletion and mitigate the CO_2 emissions in the atmosphere [1]. The thermochemical conversion routes for biomass conversion include combustion for thermal energy generation, pyrolysis for the production of bio-oil and bio-char, liquefaction (mainly for wet biomasses) and gasification for the production of Syngas.

Several biomass resources can be used in gasification reactors, such as woody biomasses or municipal solid wastes, which can be attractive for wastes reduction and valorisation [2] [3]. Biomass gasification allows to convert biomass into Syngas mainly composed of CO and H_2 [4]. These two molecules can be used afterwards as starting blocks for bio-fuel synthesis in processes such as Fischer-Tropsch catalytic synthesis [5]. Biomass gasification is a generic term encompassing several reactions occurring during the biomass conversion. The biomass gasification includes the biomass drying, pyrolysis and residual char gasification steps. The char gasification is the rate limiting step in biomass gasification reactors.

Biomass char is a porous, carbonaceous, non-organised material. It contains mainly carbon and in lower proportions, oxygen, hydrogen, nitrogen and mineral species such as potassium, calcium, sodium, silicon and magnesium. In biomass gasifiers, the char gasification reaction may take place with O_2, H_2O, CO_2, and H_2 following the reaction of combustion, steam gasification, Boudouard reaction and methanation. The gasification reaction is a heterogeneous reaction involving the reactant gas diffusion inside the char, reaction on the char active sites and diffusion of the gas product out of the particle. The reaction can be also catalysed in the presence of minerals such as potassium [6].

Hence, the char porosity, its structural features, the nature of the surface functional groups as well as the presence of catalytic minerals affect its reactivity toward the reactant gas(es). These different char properties affecting the reactivity can be classified in three categories:

- The char textural properties related to the char porosity and pore size distribution

* Corresponding author.
E-mail address: mejdi.jeguirim@uha.fr (M. Jeguirim).

- The char structural properties related to the char carboneaceous structure and graphitization (ordering)
- The char chemical properties related to the surface functional groups as well as tp the catalytic mineral species

Several studies showed that the char morphology and texture impact the gas diffusion inside the particle. For instance, Avila et al. found correaltions between the reactivity and morphology of 10 biomass chars [7]. They observed that biomasses giving the thickest walled char had the lowest reactivities, while those having the thinnest walled char had the highest reactivities. The authors related their observations to the different resistances to mass and heat transfer in the two char types. Several studies showed that the initial porosity and Total Surface Area (TSA) of chars depend significantly on the pyrolysis conditions (temperature pressure and heating rate) [8]. Indeed, Mermoud et al. observed that high heating rate chars, exhibiting a higher reactivity, have a higher pore volume consisting mainly of mesopores and macropores, while low heating rate chars exhibit a lower pore volume mainly consisting of micropores [8]. Nevertheless, attempts to correlate the initial reactivity (e.g. at a conversion ratio of 5%) of the different chars with their respective TSA were unsuccessful. The authors found that the mesopore and macropore areas are better indicators of the char reactivity.

The textural properties of chars are also strongly modified during the gasification, a noticible increase of porosity and surface area can be observed during the gasification reactions [9] [10] [11]. Reactivity of biomass char can increase up to 10 folds at the end of the reaction compared to the initial stages [12] [6]. This reactivity increase can not be related exclusively to the increase of the TSA, as evidenced by Fu et al. [13]. The authors investigated the evolution of textural and chemical features of a rice husk char during steam gasification and found that the highest TSA was obtained for a conversion of 49%. TSA decreased beyond this conversion level, probably because of pore coalescence and collapsing, but reactivity did not. Similarly, Laine et al. [14] observed that coal chars with nearly the same TSA, have different reactivity. The authors found that the Active Surface Area (ASA), determined by O_2 chemisorption on the char surface at 200–300° C [14,15], is more representative of the reactive surface. Laine et al. measured the evolution of the TSA and ASA of chars during combustion with oxygen and showed the high difference that exists between TSA and ASA [14]. The ASA was found to represent a small fraction of the TSA. Therefore, not all the char surface participates to the gasification reaction. The char Surface Functional Groups (SFG) constitute the reactive sites in the biomass char. A qualitative and quantitative analysis of the char SFG can be done by Temperature Programmed Desorption and gas analysis by Mass spectrometry (TPD-MS) [16–19]. This technique consists of heating the char sample in a high vacuum at a low heating rate. The decomposition of the SFG leads to the emission of CO_2, CO, H_2O and H_2 in a major part. The nature of the char SFG can be determined by analysing the gas emission profiles. Figueiredo et al. [16] or Zhuang et al. [18] used this technique to follow the evolution of coal char functional groups during oxidation with O_2, while Klose and Wolki [19] measured the evolution of the CO surface complexes for CO_2 and H_2O gasification reactions.

The char structure has also an impact on the char reactivity. Char structural ordering is promoted at high temperatures and long soaking time. The more ordered is the char structure, the lower is its reactivity as showed in Ref. [20]. In fact, Asadullah et al. [20] found that the reactivity to oxygen of chars obtained from a mallee wood decreases with increasing the temperature from 700° C to 900° C. The increase of temperature was accompanied by a loss of oxygen functional groups and an ordering of the char. The high levels of oxygen content in biomass fuels foster cross-linking of the carbon chains and inhibits ordering of the char matrix [21]. The loss of oxygen and hydrogen by elimination of functional groups are clear indicators of subsequent coalescence, ordering and rearrangement of aromatic rings. Tay et al. [22] studied the structural features of partially gasified char in different atmospheres containing H_2O, CO_2 and O_2 gasifying agents using FT-Raman spectroscopy. The authors found that the presence of H_2O during gasification at 800° C plays a decisive role in the evolution of char structure, in particular by decreasing the relative ratio of the small to large aromatic ring structures in the char. Keown et al. [23] made similar observations and found that the structure of cane trash chars changes drastically after contact with steam. Li et al. [24] also studied the evolution of the char structure during gasification with CO_2, H_2O and their mixtures using FT-Raman spectroscopy. The structural changes were different in CO_2 and H_2O atmospheres, char obtained in mixed atmosphere had a structure close to that obtained in H_2O atmosphere. The authors concluded that CO_2 and H_2O gasification reactions follow different pathways.

Another factor influencing the char reactivity is the type and concentration of minerals in the char. Some minerals highly impact the char reactivity as they can catalyse or inhibit the gasification reaction. For instance, K, Ca and Na were found to be catalytic species while Si and P were shown to inhibit the gasification reaction [12,25–30]. The mineral species can migrate during the reaction and form cluster or stay evenly dispersed throughout the char particle [31]. Henriksen et al. [25] showed that the presence of Si hinders the gas from penetrating into the char particle. Si was found to form clusters and block the pore access to the reacting gas. More recently, Dupont et al. [12] found that the char reactivity towards steam can be expressed as the product of kinetic term accounting for temperature and steam partial pressure dependence, and an empirical correlation bearing the concentration of K and Si. In the continuity of the their researchs on the correlation between certain mineral species concentration and the char reactivity, Hognon et al. [27] as well as Dupont et al. [6] also showed that the evolution of the char reactivity during gasification is related to the K/(Si + P) ratio.

This brief litterature overview shows that the char reactivity is highly conditioned by the its textural, structural and chemical properties. These characteristics are also highly coupled which makes the task of understanding the gasification reaction mechanisms even more difficult. Several studies focus on the modeling of the char gasification reaction in order to determine the reaction kinetic parameters [32] [33]. Char gasification models are often semi-empirical ones, as they include a term accounting for the changes in the different char properties along the gasification [34], which reflect the ambiguity of this issue. The present work aim at obtaining new insights on this issue by using a deep characterization of the char surface chemistry, structural and textural properties as well as mineral species behaviour during biomass gasification in CO_2, H_2O and CO_2/H_2O mixture.

2. Material and methods

2.1. Char preparation

The raw biomass samples are beech wood spheres with a diameter of 20 mm. Proximate and ultimate analysis of the raw wood are shown in Table 1. Low Heating-rate chars were prepared by pyrolysing the wood spheres under nitrogen in a batch reactor. The wood spheres were placed on a metallic plateau, spaced enough to avoid chemical and thermal interactions. The plateau was introduced in the furnace heated zone which was progressively heated from room temperature to 900° C at 5° C/min. The chars

Table 1
Proximate and ultimate analysis of the raw beech wood (% dry basis).

Proximate analysis			Ultimate analysis			
VM	Ash	FC	C	H	O	N
88.1	0.4	11.5	46.1	5.5	47.9	0.1

were kept for 1 h at the final temperature, cooled under nitrogen and stored afterwards in a sealed recipient. The low heating rate ensure a good temperature uniformity in the wood particle and leads to a quite homogeneous wood-char, from the structural and chemical viewpoints [8,25,35]. With high heating rates there can be heterogeneity among the char layers from the surface to the particle centre due to the temperature gradient and heat transfer limitations during the pyrolysis stage. After the pyrolysis reaction, the char particles shrink and get an ovoid form. The mean particle diameter, calculated as the average of the three particle dimensions was estimated at 13 mm.

Some of the char particles were afterwards ground with a mortar and a pillar. Char particle having size of 0.2 mm were retained for gasification experiments at 900° C. To ensure of the chemical and structural homogeneity of the char particle, the char structure and chemical composition were analysed at three location: at the surface, at half the distance from the centre and at the centre. Disparities in the elemental composition and Raman signals from the core to the char surface were negligible and showed that the char sample is homogeneous [36].

2.2. Char gasification experiments

The Macro-Thermogravimetry experimental device is described in details in Ref. [37]. The apparatus consists of a 2 m long, 75 mm i.d. alumina reactor which is electrically heated, and a weighing system comprising an electronic scale having an accuracy of ±0.1 mg. A metallic stand holding a 1 m long, 2.4 mm external diameter hollow ceramic tube is placed on the electronic scale. The ceramic tube hold the 5 cm diameter platinum basket in which the biomass particles are placed. The gas flow rates are controlled by means of mass flow-meters/controllers. The gas flow inside the reactor is laminar and its average velocity is 0.20 m/s.

For gasification experiments, a wood-char mass of 130−150 mg is spread-out on the whole surface of the 50 mm diameter platinum basket in the form of a thin layer. The surface of the crucible is large enough to allow spreading this mass in the form of a thin layer. The char is directly exposed to the surrounding atmosphere as the platinum basket is simply a circular plane without any side wall. The crucible is introduced in the furnace under a nitrogen flow. The char is kept 5 min under nitrogen before starting the gasification. During this period, the char loses mass in the form of water vapour and light gases. This mass loss was estimated to be less than 6% of its initial mass. This duration is sufficient for the establishment of a thermal and mechanical equilibrium between the weighing system, the furnace and the surrounding gases. Once a constant mass is displayed on the electronic scale, the gasification medium is introduced and the reaction starts. The gasification reactions were performed at 900° C with 20% H_2O, 20% CO_2 and 20% H_2O + 20% CO_2 in nitrogen.

The char conversion level is given by:

$$X_{(t)} = \frac{m_0 - m_{(t)}}{m_0 - m_{ash}} \quad (1)$$

Where m_0, $m_{(t)}$ and m_{ash} are the initial mass of char, the mass at a time t and the mass of the residual ash, respectively. The char reactivity was calculated over time following the relation:

$$R_{(t)} = \frac{1}{1 - X_{(t)}} \times \frac{dX_{(t)}}{dt} \quad (2)$$

To follow the evolution of the char properties during the gasification reaction, partially gasified chars were prepared at 20%, 50% and 70% of conversion. Knowing the initial char mass that was introduced in the crucible, the gasification reaction was stopped after reaching the desired conversion level. The gasifying medium flow was directly switched to pure nitrogen and the platinum basket bearing the sample was quickly pulled out toward the reactor colder zone at a temperature near to 180° C. The reacted char was kept in this zone during 4 min to cool before taking it out directly to the ambient atmosphere. Afterwards, the chars were preserved in sealed recipients under nitrogen to avoid chemical transformations of the surface functional groups in air.

In the following sections, the char sample name will be composed by the sequence: 'gasifying agent'-'level of conversion'. For instance, the 'CO_2-X50' char sample refers to the char sample obtained after CO_2 gasification up to 50% of conversion. The pristine char (X = 0) is named Ref-char.

2.3. Char surface chemistry analysis

The char surface chemistry was investigated via the TPD-MS technique. The TPD-MS experimental bench comprises a quartz tubular reactor electrically heated in which is introduced a quartz crucible containing nearly 20 mg of char, a pumping system to create vacuum and a mass spectrometer for gas analysis. After introducing the char sample in the reactor, the reactor is sealed and outgassed down to 0.013 Pa of pressure by means of a turbo-molecular pump. The sample is afterwards heated up to 900° C at constant rate of 5° C/min and kept at this final temperature during 1 h. During the analysis, the functional groups are removed from the char surface, which results -depending on the nature of the functional groups-in the emission of H_2O, CO_2, CO and H_2 [16,17]. The gases resulting from the SFG decomposition were continuously quantified by a mass spectrometer, which is calibrated for H_2, CO, CO_2, H_2O and N_2. The total pressure of the gas released during the heat treatment was also measured using a Bayard Alpert gauge. This allows performing a mass balance by comparing the sum of partials pressures obtained from the MS analysis with the pressure recorded by the Bayard Alpert gauge. The total amount of each gas released was computed by time integration of the TPD-MS curves.

2.4. Char structural properties

Raman spectroscopy was used to study the structure of the chars during gasification. This technique can provide information about an 'average structural composition' of the chars and thus allows a comparison between the different char sample at the different conversion levels. Raman spectra of the chars were recorded with a BX40 LabRam, Jobin Yvon/Horiba spectrometer. Several char particles were sampled and deposited on a rectangular glass slide for the Raman analysis. Raman spectra were obtained by a backscattered configuration with an excitation laser at 635 nm. The Raman spectra were recorded at 6 locations of the char sample. Mean values as well as relative standard deviations were calculated for the different parameters, taking thus into account the heterogeneity among the char sample. For disordered carbons, the Raman spectrum is thought to be the combination of several bands corresponding to different carbonaceous structures. It is often considered as the results of five signals corresponding to five carbonaceous structures [38−42]:

- The G band at 1590 cm^{-1}: stretching vibration mode with E2g symmetry in the aromatic layers of the graphite crystalline [39].
- The D1 band at 1350 cm^{-1}: graphitic lattice vibration mode with A1g symmetry and in-plane imperfections such as defects and hetero-atoms.
- The D2 band at 1620 cm^{-1}: lattice vibration similar to that of the G band. The D2 band results from graphene layers which are not directly sandwiched between two other graphene layers. Sheng [40] reported that the D2 band is always present when the D1 band is present and that its intensity decreases with the increase of the degree of organization in the char.
- The D3 band at 1500 cm^{-1}: Related to amorphous carbon structures and appears as a very broad band. It is suggested to originate from the amorphous sp^2-bonded forms of carbon (organic molecules, fragments or functional groups, in poorly organised materials).
- The D4 band at 1200 cm^{-1}: appears only in very poorly organised materials, such as soot and coal chars [39,40]. It is attributed to sp^2 - sp^3 mixed sites at the periphery of crystallites and to C−C and C=C stretching vibrations of polyene-like structures.

The D3 and D4 bands are suggested to be the major reactive sites in the char and thus related to the char reactivity. The deconvolution procedure was performed with a MATLAB [43] program based on the work of Haver et al. [44]. Spectrum fitting was performed following a least square minimization procedure between the raw signal and the calculated one. The Raman signal was deconvolved into 5 bands. Assuming a Gaussian shape for the different bands, their positions were fixed to the above mentioned values. The height and width of the different bands were determined in a way to best fit to the experimental signal.

2.5. Textural properties and surface morphology of the chars

The textural properties of the chars were investigated with a Micromeritics ASAP 2020 instrument using N_2 adsorbate at 77 K. Prior to the analysis, the char samples were out-gassed overnight in vacuum at 300° C. The Total Surface Area (TSA) was calculated from the BET equation in the relative pressure range of 0.05−0.15 while the micropore volume V_{micro} was estimated by using the α_s method. The mesopore volume V_{meso} was obtained by subtracting the micropore volume from the total pore volume of N_2 adsorbed at a relative pressure of 0.95. The pore size distribution was determined using the DFT model for carbon slit pores with a finite depth [45]. Scanning electron microscopy (Philips model FEI model Quanta 400 SEM) and energy dispersive X-ray spectrometry (EDX) were used to observe the morphology and the surface elemental analysis of the prepared chars, which allows determining the elemental mapping of the samples.

2.6. Concentrations and behaviours of minerals in the chars

The concentrations of several minerals in the different chars was measured by X-ray fluorescence spectrophotometry using a PHILIPS PW2540 apparatus equipped with a rhodium target X-ray tube and a 4 kW generator. About 100 mg of char were ground and mixed with 200 mg of boric acid, and then pressed into a pellet under a 9 tons pressure for 45 min. The use of boric acid is required to pelletize the char powder since the char has a hydrophobic character and could not be densified without a binder. The acid boric signal is easily eliminated during the XRF analysis. The behaviour of some major mineral species during gasification was analysed using the elemental mapping obtained during the SEM-EDX analysis.

3. Results

3.1. Evolution of the char reactivity

The char reactivity in 20% CO_2, 20% H_2O and their mixture at 900° C is shown in Fig. 1. The char reactivity towards H_2O is nearly twice faster than its reactivity towards CO_2. The char reactivity in 20% CO_2 + 20% H_2O atmosphere is higher than its reactivity in 20% H_2O atmosphere, denoting the non-inhibiting character of CO_2 when it is co-reacting with steam in such operating conditions. The char reactivity in mixed atmospheres can be fairly described by adding the reactivities obtained in single atmospheres as shown by the dashed line curve in Fig. 1. The experimental mixed atmosphere reactivity is slightly higher than the one obtained by the additive law. However, the approximation is reasonable as this latter is located in the standard deviation zone of the experimental results.

Previous calculations for single atmosphere gasification experiments (20% CO_2 or 20% H_2O in N_2) showed that in these conditions of temperature and char particle size, external as well as in-bed diffusional limitations can be considered as negligible. However, modelling results based on the Thiele modulus approach showed there are slight internal diffusional limitations in single atmospheres (effectiveness factor = 0.92) which would be accentuated when mixing the two gases [36]. In the present cases, the char reactivity would be slightly affected by internal diffusional limitations, especially in the first stages of the reaction for which the porosity is not well developed.

3.2. Evolution of textural properties

3.2.1. Surface morphology

Despite its limited resolution at the micrometer level, SEM imaging allows a direct visualisation of the char surface morphology during gasification. SEM images bear valuable information on the state of the char surface as well as on the development of macroporosity. For the non-gasified char (Fig. 2), SEM images at the level of cells show a quite smooth surface with the presence of mineral particles evenly dispersed (proven by the EDX analysis).

Considering CO_2 gasification, we observed that the gasification reaction affected almost all the surface in an equivalent way (Fig. 3). Alteration of the char surface is observed at the cell level as well as on its surroundings. The char surface shows clearly an higher porosity development along the gasification. The char gets a spongelike surface at an advanced gasification conversion.

In the case of H_2O gasification, some differences in the char surface morphology were noticed in comparison with CO_2

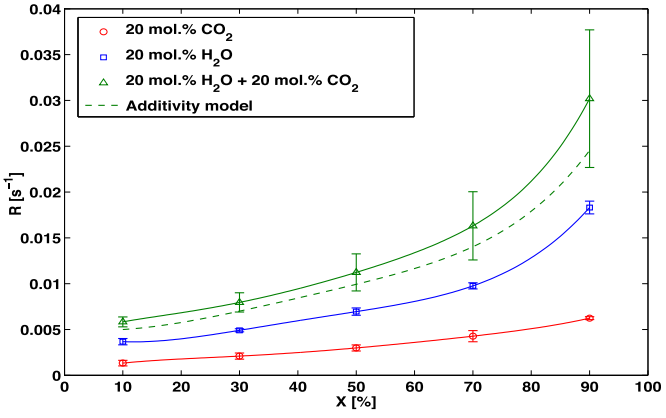

Fig. 1. Char reactivity in 20% CO_2, 20% H_2O and their mixture at 900° C.

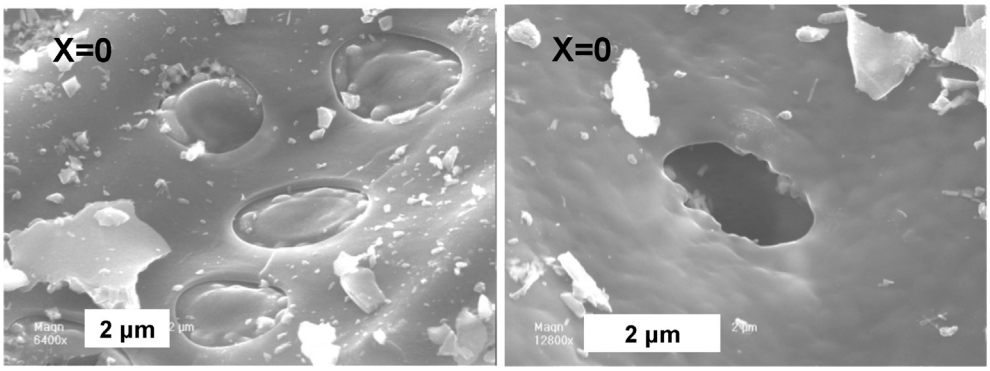

Fig. 2. SEM images of the pristine char.

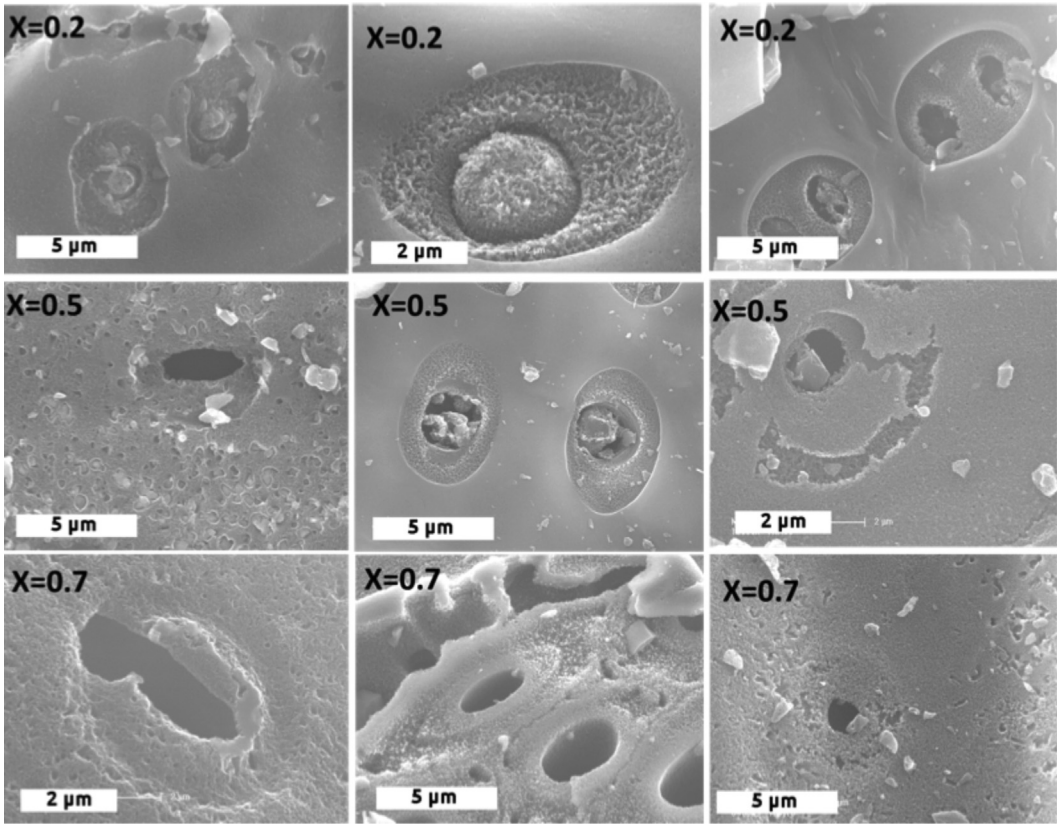

Fig. 3. SEM images of the char along gasification in left:CO_2, centre:H_2O and right:mixed atmosphere.

gasification. At 20 and 50% of conversion, the char surface was altered at the level of cells and their near periphery while the rest of the surface was almost as intact and smooth as that of the non gasified char. It is only at X = 0.7 that the char surface was seen to be highly affected by the gasification with H_2O.

This difference between the char surface morphologies observed respectively in CO_2 and in H_2O gasification suggests a limited diffusion for CO_2 molecules inside the char particle and an accentuated surface reaction, while H_2O, which has a better diffusivity and a smaller molecular size, would get inside the char matrix and have a more developed volumetric reaction.

Information on micro and mesopores, which are unobservable using the SEM, are unavailable. Nevertheless, one can suspect a high microporosity at the cell surroundings in which H_2O can diffuse and reacts, while it would be inaccessible to the CO_2 molecules which react mainly at the external surface causing its alteration.

The mix-char show a texture at X = 0.2 similar to that obtained under H_2O with a porosity mainly appearing around the cell region. At X = 0.5, we observed the alteration of the external surface probably due to CO_2 gasification. As for the two precedent char, at X = 0.7, the char surface was quite well damaged with a marked spongy-like morphology.

3.2.2. Surface area and porosity

Fig. 4 shows the N_2 adsorption isotherms (left) and pore size distributions(right) of the ref-char, CO_2-chars, H_2O-chars and Mix-chars along the conversion. The adsorption isotherms are presented in log scale to show the low pressure data which correspond to the N_2 adsorption in micropores.

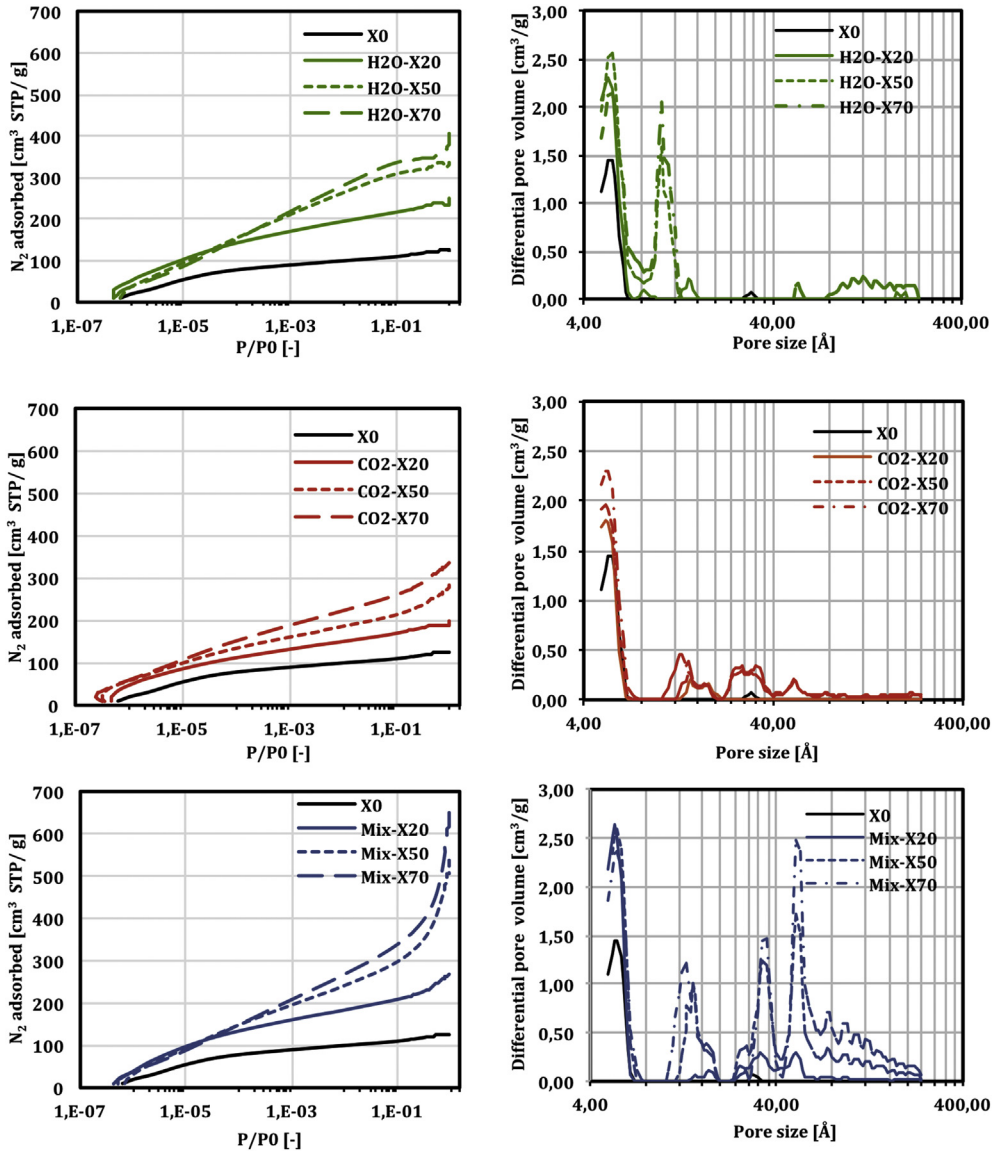

Fig. 4. Right: N_2 adsorption isotherm of the CO_2-chars, H_2O-chars and Mix-chars along the conversion, and left: corresponding pore size distributions according to DFT model.

The N_2 uptake increases with the extent of conversion for all chars indicating the extension of porosity due to the gasification reaction. The isotherms are close to the type I for all the chars obtained in CO_2 and H_2O, indicating that they are almost microporous and that the TSA resides mainly in the micropores [46,47]. Moreover, the conversion up to 20% leads to the increase of the adsorbed volume over the whole relative pressure range 10^{-7} 10^{-1}. This corresponds to the development of all pore sizes between 0 and 2 nm. For $X > 20\%$, the development of porosity proceeds mainly through the increase of the larger micropores ($10^{-4} < P/P_0 < 10^{-1}$) while the ultra-micropores are only slightly modified. For an equivalent conversion level, the N_2 volume adsorbed in micropores for H_2O-chars is higher than for CO_2-chars. This indicates that the gasification with H_2O is more volumetric than CO_2 gasification which confirms the SEM observations. H_2O molecules would diffuse much more easily inside the char matrix than CO_2 molecules which react more on the surface. Furthermore, H_2O-chars show the presence of mesopores especially at 50% and 70% of conversion where the adsorption and desorption isotherm show hysteresis loops (P/P_0=0.421). Beyond 50% of conversion, an enlargement of the porosity is noticed for H_2O gasification.

For the three atmospheres, the TSA increases almost linearly with the conversion (Table 2). At equivalent conversion levels, the TSA of CO_2-chars is always lower than that of the H_2O-chars. At X = 70%, the TSA of the char is higher than 1000 m^2/g regardless of the atmosphere composition.

The PSD of all chars are shown in the left had-side of the Fig. 4. It can be noticed that for $X > 20\%$, there is a development of ultra-micropores (size below 8 Å) in the three atmospheres. The development of such a narrow microporosity with the extent of reaction in the three atmospheres demonstrates the presence of internal

Table 2
TSA evolution along the conversion for the three gasification reactions.

Conversion level (%)	0	20	50	70
TSA in H_2O gasification (m^2/g)	437	866	1225	1334
TSA in CO_2 gasification (m^2/g)	437	669	842	1028
TSA in CO_2 + H_2O gasification (m^2/g)	437	824	1174	1332

diffusional limitations during the gasification reactions even at higher conversion levels.

Beyond 20% of conversion, one can notice the development of 11 Å micropores in the case of H_2O gasified chars, while one can observe the formation of larger micropores and of small mesopores for the CO_2 gasified chars in the pore size range of 10–40 Å. Also, it can be observed that large mesopores (76–220 Å) are developed in the case of H_2O gasification, but not visible in the case of CO_2 gasification.

Mix-chars are also highly microporous. The increase of the micropores widths with conversion can also be noticed. The isotherms show also a hysteresis loop denoting the presence of mesopores which are due most probably to steam gasification. The Mix-chars exhibit a higher pore volume than the single atmosphere chars for equivalent conversion levels. This underlies that the gasification reaction occurs in a more volumetric way in mixed atmospheres than in single atmospheres. Similar observations were made by Roman et al. [48] during the physical activation of olive stone chars with CO_2, H_2O and their mixture. The authors found that the porosity developed in steam gasification was higher than that obtained in CO_2 gasification. They also observed that simultaneous use of CO_2 and H_2O resulted in a high volumes of pores, suggesting a synergistic effect when mixing the two gases.

A worthy fact is that the Mix-chars show a pore size distribution similar to that of the CO_2 chars (bimodal distribution), however the pore volume is much more developed in mixed atmosphere gasification. What is also curious in the PSD of Mix-chars is the absence of the 11 Å micropores developed in the case of steam gasification, and the development of larger micropores and small mesopores respectively in the wider ranges of 10–20 Å and 30 to 50 Å. It can be also observed that the larger mesopores are more developed in mixed atmosphere gasification.

Keeping in mind that this bimodal pore size distribution was observed for CO_2 gasification, a plausible explanation to these observations may be formulated: in mixed atmosphere gasification, H_2O molecules would facilitate the CO_2 molecules diffusion to the 11 Å pores. CO_2 molecules can then react on and induce their widening. In a similar way, for the 10 to 20 Å and 30 to 50 Å pores, it would be an enhanced CO_2 diffusivity inside this porosity in the presence of H_2O, which induce their much pronounced development by CO_2 gasification.

Owing to these results, there can be a synergy between the two molecules for the access to the internal surface area of the char. On one hand, CO_2 and H_2O can compete for the same active sites, which tends to lower the reaction rate, while in the other hand, H_2O can facilitate the CO_2 diffusion to other active sites, which tends to increase the reaction rate. These results indicate that the situation of mixed atmospheres is likely more complicated than the simple case of an additive law denoting the reaction on separate active sites.

3.3. Evolution of char structure

Raman spectra of the char samples were well represented by the five gaussian bands deconvolution procedure. An example is given in Fig. 5. Over the 60 fitted spectra, the highest relative mean error obtained following this fitting procedure was 3%. The ratios between some major band intensities were used to investigate the char structure evolution during the gasification with CO_2, H_2O and mixture of the gases. The different peak intensity ratios are plotted in Fig. 6.

For instance, when considering the ratio between the D3 band intensity and D1 band intensity I_{D3}/I_{D1}, one can observe that this ratio is almost constant along the gasification reaction with CO_2. On the contrary, in a H_2O containing atmosphere this ratio decreases markedly denoting the preferential reaction of H_2O with the D3

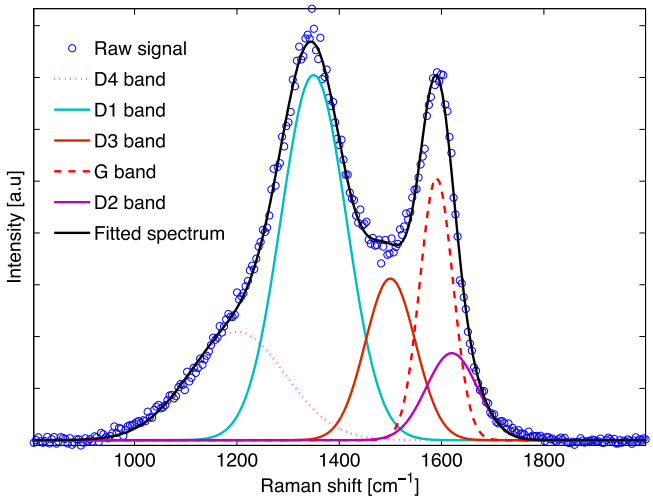

Fig. 5. Example of Raman fitted spectrum.

type carbonaceous structures (organic molecules, fragments of functional groups and amorphous sp^2 carbon forms), and/or the growth of small rings to bigger ones of D1 type due to H radicals generated by H_2O gasification. These H radicals can penetrate into the char matrix and induce the ring condensation. Both phenomena can induce the observed decrease in the I_{D3}/I_{D1} ratio.

The ratio I_{D3}/I_G is constant along the conversion for the CO_2 gasification while it decreases in a H_2O containing atmosphere. Similar results are reported in the literature on the drastic change of the char structure upon contact with steam [23,24]. The Mix-char structure evolution is similar to that of H_2O-char. This similarity can be due to the preponderance of steam gasification reaction in the global carbon gasification process. I_{D1}/I_G increases during the CO_2 gasification denoting the reaction of CO_2 with G type carbons and/or the condensation of small rings into bigger ones of D1 type. However, the trend was in the opposite way for the H_2O gasification, showing the different reaction pathways for the CO_2 and H_2O gasification reactions.

I_{D4}/I_G shows a decreasing trend for X<50% in the case of H_2O gasification, while it increased a bit at X=70% compared to the value obtained for the raw char, in the case of CO_2 gasification. At equivalent conversion levels, I_{D4}/I_G was at higher values in the case of CO_2 gasification compared to H_2O gasification. For the mix-char, the trend was to a slight decrease and the values were located between those obtained in the single atmosphere cases. The D4 band is thought to represent sp^2-sp^3 sites at the periphery of crystallites and/or C–C, C=C polyene-like structures. These structures seem more reactive in the presence of H_2O than in the presence of CO_2.

I_{D2}/I_G evolution was similar for the three chars. This ratio increased along the gasification denoting the increase of the proportion of graphene layers which are not sandwiched between two other ones.

Altogether, these data shows that CO_2 and H_2O reactions would follow different pathways. Also, the results obtained for Mix-chars indicate that steam greatly influence the char structure, which tends towards that of H_2O chars. This would be related to the predominance of the steam gasification reaction over the CO_2 gasification reaction in the case of mixed atmosphere gasification.

3.4. Mineral species

3.4.1. Concentration and behaviour of minerals

The molar concentrations of the main minerals found in the

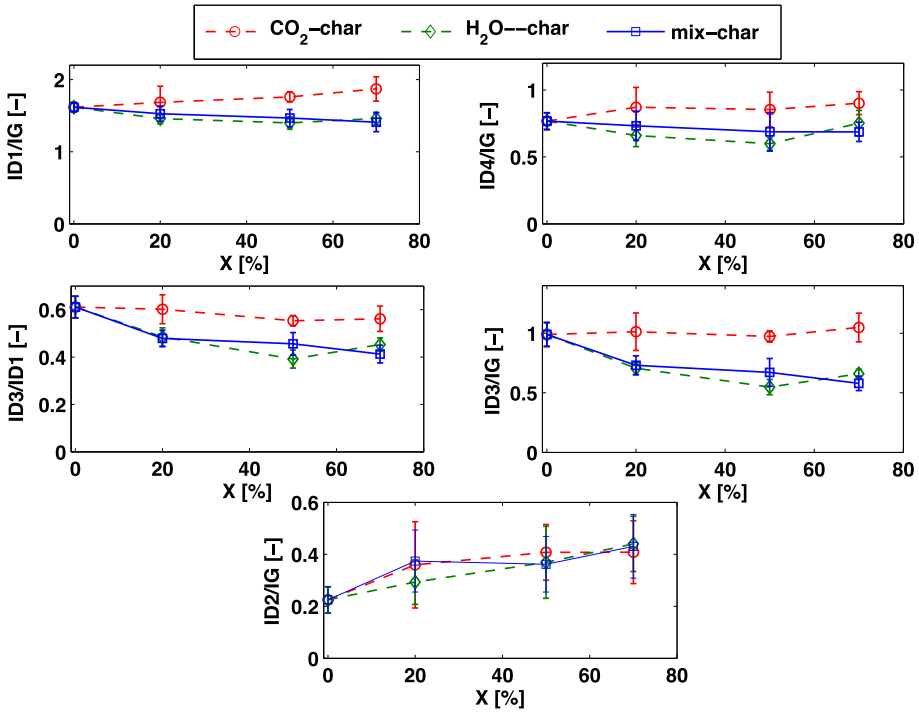

Fig. 6. Peak intensity ratios evolution during the char gasification in CO_2, H_2O and their mixture.

chars are shown in Fig. 7. The mineral phase of the char after pyrolysis is mainly constituted by Alkali and Alkaline Earth Metals (AAEM) which represent near to 60 mol.% of the minerals. These species are, in order of decreasing concentration: K, Ca and Mg. The Ref-char contains also transition metals such as Zn, Mn and Fe and non-metals such as Si and P.

K, Ca, Mg and P concentrations globally increase along the gasification with CO_2, while that of Al and Zn decrease since the early stages of gasification. Besides, for Fe and Si, their concentrations is relatively constant along the reaction. An increasing concentration along the reaction indicates a higher retention in the char while a constant one or a decreasing one indicates that the specie is being rather volatilized. Similarly as for the CO_2 gasification, the concentrations of AAEM as well as that of P increase during H_2O gasification. One can observe that K, Ca and Mg retention is higher in H_2O atmosphere than in CO_2 atmosphere which would impact the char reactivity due to the catalytic activity of these species. Zn concentration decreases drastically since the very beginning of the reaction as for CO_2 gasification. Al and Fe concentrations increase, which is different from the case of CO_2 gasification. One can also notice that Si is more retained in the char than in the case of CO_2 gasification. Silicon would volatilize in the presence of CO_2 while it remains in the char matrix in the case of steam gasification. This is an important observation since Si is

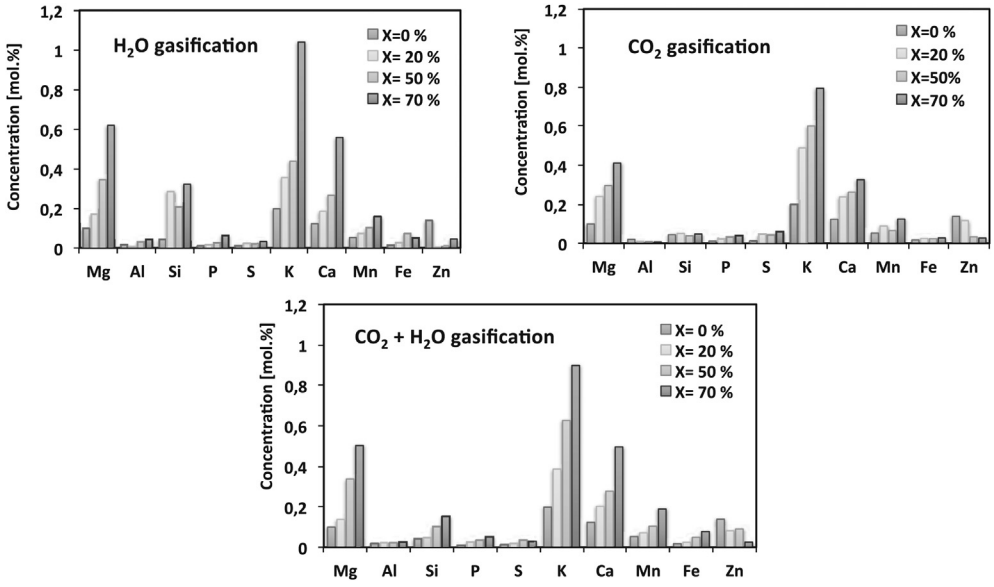

Fig. 7. Molar concentration of minerals in the char (mol.%) along the gasification with H_2O, CO_2 their mixtures.

known to be an inhibitor of gasification.

In mixed atmosphere gasification, one can observe a kind of "intermediate results" lying between those obtained in single atmospheres, denoting the action of H_2O and CO_2. Si and Al are less retained when CO_2 is injected with H_2O. Also, Zn concentration decreases less drastically in the presence of CO_2 along with steam.

SEM observations coupled to EDX analysis revealed interesting information about the behaviour of major minerals contained in the chars (data not shown). K and Mg were found to be present in a very diffuse state in the char matrix while Ca was found in the form of big clusters located at the char surface. Similarly, Si was found in the form of big clusters located at the entry of pores. The clusters were seen to contain a mixture of metals, and high concentrations of oxygen are present, indicating that the minerals are in the oxide or carbonate forms. These results are in accordance with the findings of [49]. Dispersion of minerals as well as their nature and concentration play a crucial role in the heterogeneous gasification reactions [28].

3.4.2. Relationship between minerals and char reactivity

The abundance of mineral species in the char is of high importance as some of them (mainly AAEM species) play a well admitted catalytic role in H_2O and CO_2 gasification [12,27,50]. K, Ca, Mg constitutes active sites on which gasification occurs via several steps including carbonation, de-carbonation and formation of metal oxides among others [28]. While catalytic active species concentrates into the char, the number of active sites increases consequently which may explain the increasing char reactivity along conversion. Other species inhibit the gasification reaction such as Si and P [6,12,27]. Recently, some authors found a correlation between the K/Si ratio and the char reactivity with CO_2 at conversion levels higher than 0.6 [30]. The char reactivity would be thus correlated with some mineral species concentrations. We analysed the possible correlations and found that there were effectively ones for some minerals.

Fig. 8 shows the evolution of the char reactivity with the concentrations of K, Ca and Mg for the different gasification atmospheres. Near linear correlations were found between the char reactivity and the molar concentrations of these species for the different atmospheres.

Similar results were obtained by Ref. [51]. The authors gasified chars from 14 different biomass samples including sawdust, bark and some agricultural wastes under 50 kPa steam at 850° C. The authors found linear correlations between the reactivity at X=0.5 and the sum of K, Na and Ca. They observed that the alkali metals are more effective than Ca. For biomasses with high Si content (rice husks and bagasse), the authors observed much lower reactivities. They assumed that the formation of alkali silicates at low temperatures curtailed the catalytic action of K.

Mermoud et al. [8] found also linear correlation between the initial gasification rate of beech wood char and its ash content. In a more recent study, Hognon et al. [27] reported two typical behaviour of biomass char, those which reactivity decrease along the conversion having a K/Si ratio below one, and those having a K/Si ratio above one exhibiting a constant reactivity or slight decrease followed by reactivity increase beyond 70% of conversion. Si is an inhibitor of the gasification and thought to encapsulate catalytic active species such as K reducing consequently its activity.

The present results show quite interesting potential synergy between CO_2 and H_2O during gasification as the presence of CO_2 would induce the departure of Si from the char which is an inhibitor in steam gasification.

3.5. Evolution of surface chemistry during gasification

TPD-MS experiments provide interesting information on the surface chemistry of the chars (Fig. 9). The pristine char exhibits a surface chemistry which is typical of an hydrophobic material obtained by pyrolysis of a carbon precursor. The low stability surface groups are mainly carboxyles, which lead to the desorption of CO_2 at low temperature (150–300° C). These functional groups are in relatively low quantities. The main surface chemistry is composed of ether and semi-quinones which decompose to CO at high temperature [16,17]. This low CO_2/CO ratio is often observed e.g. for activated carbons [52]. The emission of water during the TPD-MS experiments is low. At moderate temperatures (below 500° C), it would related to dehydration reactions between surface groups which form lactones and anhydrides. At a higher temperature, H_2O can be emitted by the dehydration of a phenol and a carboxylic acid, leading to the formation of lactones. It can also result from the dehydration of two phenol groups forming thus an ether [16,17]. The decomposition of these groups explains in a part the emission of CO and CO_2 between 300 and 600° C. H_2 emission begins at 750° C, it is due mainly to thermal decomposition of C–H bonds.

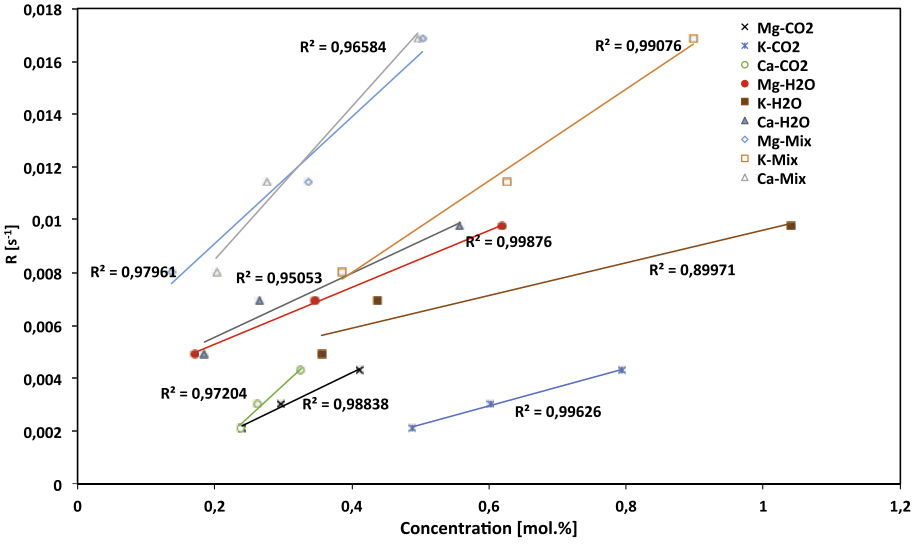

Fig. 8. Relationship between the char reactivity and molar concentration of K, Ca and Mg in the char (mol.%) along the gasification with H_2O, CO_2 and their mixtures.

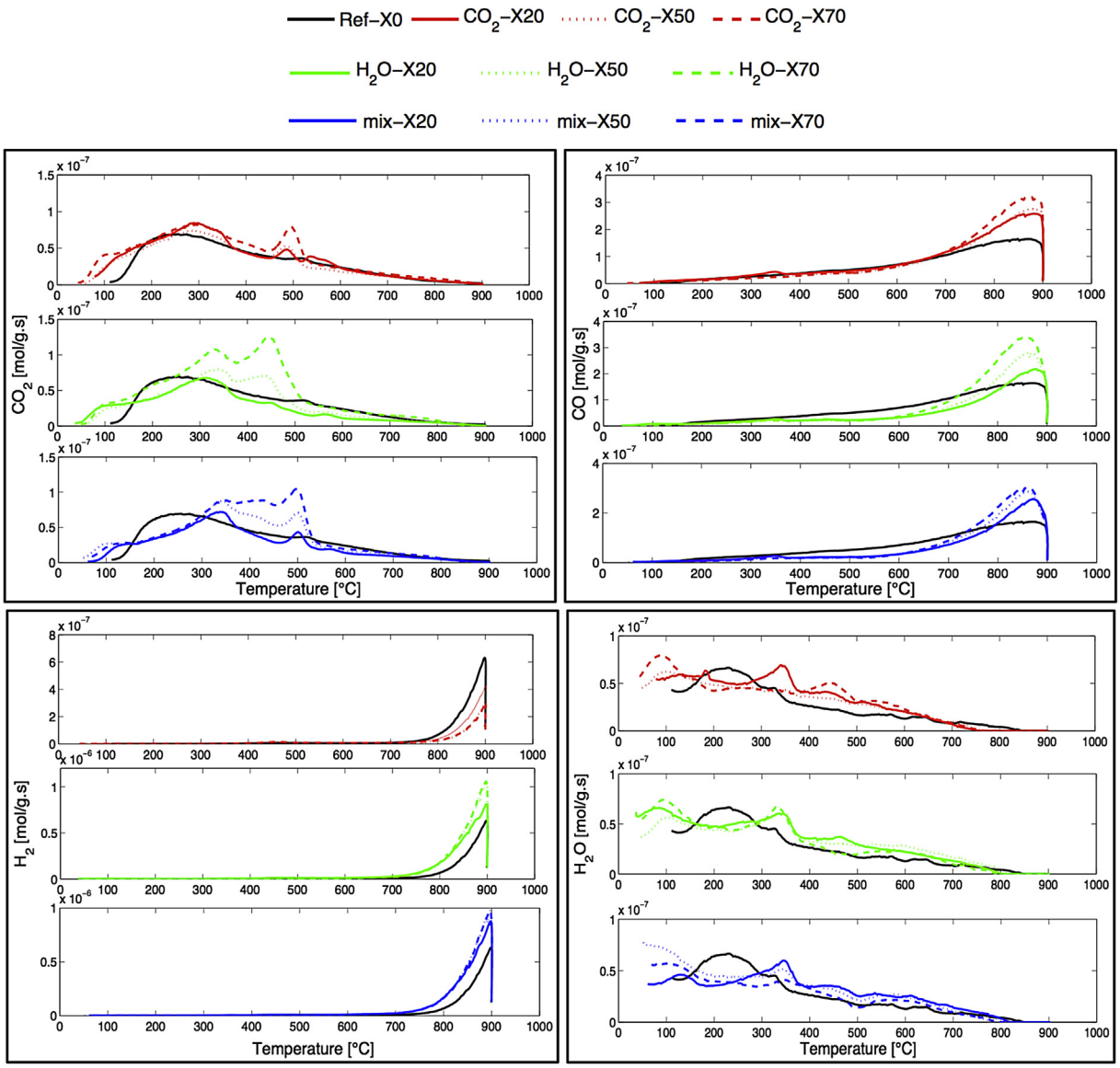

Fig. 9. Desorption profiles during TPD experiments over the char samples.

In the temperature range of 150–350° C corresponding to carboxyles decomposition, an increase of CO_2 emission is observed for CO_2-chars while a decrease is observed for H_2O-chars. At higher temperature, corresponding to anhydrides and lactones decomposition [16,17,49,53], the CO_2 emission rate increased regardless of the reacting gas composition. This results denotes an increase of acidic functions on the char surface. The increase of the intensity of this peak can be explained by the conversion of some carboxylic groups to anhydrides and lactones [53].

For the different CO_2 chars, the CO signal is nearly the same in the temperature range of 20–600° C. The variation with the conversion level are noticed beyond 600° C where the peak intensity increases with the conversion level. For all the char samples, the CO signal exhibits a single peak with a maximum at 900° C, its intensity increases with the conversion level.

It is worth-noting that the CO signal for the CO_2 chars fits well with that of the Ref-char in the temperature range of 20–600° C, while less CO is emitted between 200° C and 600° C for the H_2O-chars and Mix-chars. The functional groups emitting CO at moderate temperatures are thought to be ethers, anhydrides and phenols, while at high temperatures, quinones decomposition would be responsible of the CO emissions [17]. Thus, anhydrides and phenols may have reacted in the early stages of gasification ($X < 20\%$) in the presence of steam, explaining the observed differences concerning the CO signal. This observation can be correlated with the decrease of I_{D3}/I_{D1} and I_{D4}/I_{D1} ratios for chars gasified in the presence of steam. The D3 and D4 bands results, at least in a part, from anhydrides, ethers and phenols.

H_2 peak intensity decreased with the conversion for the CO_2 chars. Even the starting of the peak was at higher temperatures for the CO_2-X50-char and CO_2-X70-char. However, for the H_2O-chars and Mix-chars, the H_2 signal increases with the conversion. The starting of the peak was at lower temperatures (680–700° C) than for the CO_2-chars. The hydrogen on the chars gasified in presence of steam is likely less severally bonded on the surface than in the case of CO_2 gasification. Also, the peak intensity was greater for H_2O-chars and Mix-chars than for the CO_2-chars. A clear difference is thus noticed on the H_2 emissions when CO_2 is the gasifying medium. It is likely that CO_2 reacts on H sites and reduces consequently the H concentration in the char while the increasing

quantity of H_2 emitted from H_2O-chars and mix-chars is related to the continuous hydrogenation of the char surface by the steam gasification reaction.

Fig. 10 shows the evolution of the total emitted amount of H_2O, CO_2, *CO* and H_2 from the different char samples. H_2O emitted quantity increased a bit for the three chars at 20% of conversion and remained almost constant along the conversion except for the Mix-char where it decreased beyond 50% of conversion. The H_2O-char and Mix-char show a decrease in the emitted CO_2 quantities at 20% of conversion compared to the Ref-char. This can be related to the preferential reaction of H_2O with phenols, ethers and anhydride functional groups in the first stages of the reaction contributing in the CO_2 emission from the char surface as explained above.

Afterwards, the CO_2 quantity increased steadily with conversion. CO_2 and H_2O were the minor desorbed species while H_2 and CO emissions were greater by almost 1 order of magnitude. The H_2 emissions decreased with the conversion for the CO_2-char, from 1.4 μmol/g for the Ref-char to 0.83 μmol/g at 70% of conversion. On the contrary, it increased for the H_2O-char and Mix-char along the conversion up to 1.9 μmol/g at 70% of conversion. The *CO* emitted quantity was always higher for the CO_2-char than in the 2 other chars. It increased a bit from 0.8 μmol/g to nearly 1 μmol/g at 20% of conversion and remained almost constant afterwards. On the contrary, it decreased from 0.8 μmol/g to 0.6 μmol/g for the H_2O-char and Mix-char at 20% of conversion and then showed an increase trend up to 70% of conversion. These two trends concerning H_2 and CO constitute the main difference between the H_2O and CO_2 gasification reactions.

What can be noticed when having a global view on the different trends is that the gas evolution for the Mix-char followed always that of the H_2O-char. In mixed atmosphere gasification, if we consider that H_2O and CO_2 react independently, near to 70% of the char is converted by the steam gasification reaction as this latter is twice as fast as the Boudouard reaction. This may explain the fact that the mix-char TPD profiles look like that of the H_2O-char. The fact that the H_2O-chars and Mix-chars contained more H may be explained by the steam gasification reaction. Water dissociation over the char surface is at the origin of the continuous hydrogenation of the surface [54]:

$$2C() + H_2O \rightarrow C(H) + C(OH) \tag{3}$$

$$C(OH) + C() \rightarrow C(H) + C(O) \tag{4}$$

These reactions explain the formation of semi-quinones which decomposes to CO at high temperature. The emission of H_2 during TPD-MS analysis is then due to the dehydrogenation of two neighbouring C(H) or C(OH) sites following the possible reactions of:

$$C(H) + C(H) \rightarrow 2C() + H_2 \tag{5}$$

$$C(OH) + C(H) \rightarrow C(O) + C() + H_2 \tag{6}$$

$$C(OH) + C(OH) \rightarrow 2C(O) + H_2 \tag{7}$$

The decrease of in the H_2 quantities in the CO_2-chars has likely to do with the absence of hydrogenation reaction and/or reaction of CO_2 on the H sites. The fact that the CO_2-chars contain more CO emitting groups may be explained by the Boudouard reaction which is constantly providing CO intermediate species on the char surface:

$$C() + CO_2 \rightarrow C(O) + CO \tag{8}$$

$$C() + CO_2 \rightarrow C(O) + C(CO) \tag{9}$$

In H_2O gasification, intermediate surface groups are more various: C(O), C(CO), C(H) and C(OH). This is why the CO emissions are greater for the CO_2-chars than the H_2O-chars at equivalent conversion levels. The same reasoning can be held for the H_2

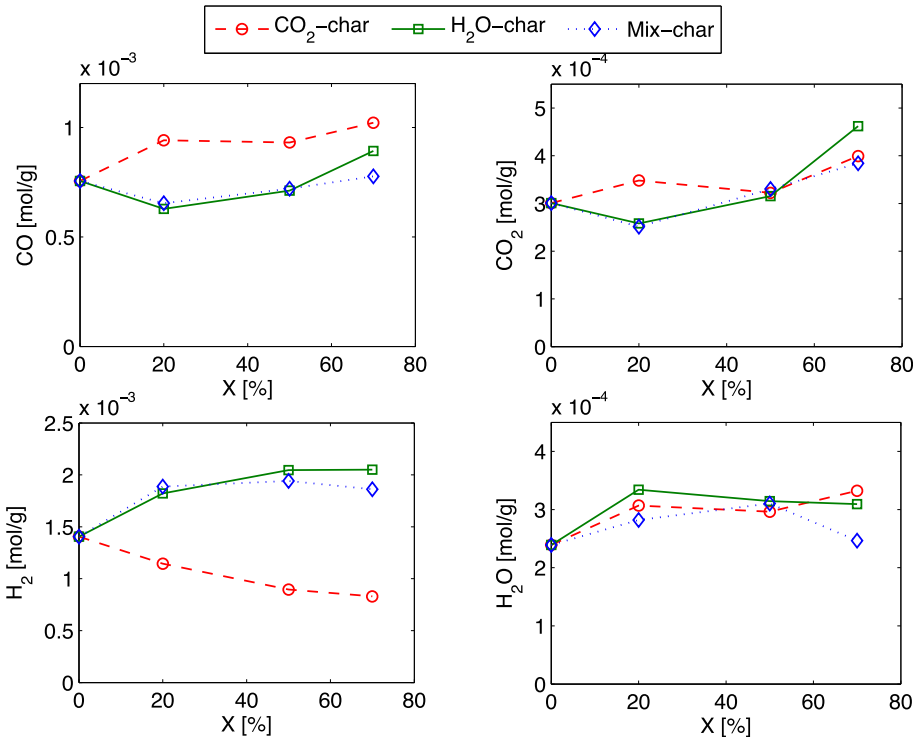

Fig. 10. Cumulated gas quantities emitted during TPD-MS experiments.

Table 3
Main differences between the gasification reactions in CO_2 and H_2O.

	H_2O gasification	CO_2 gasification
SFG	Less ethers, anhydrides and phenols since the early gasification stages Differences in peak positions compared to CO_2 gasification	More CO emitting FG Much less hydrogenated char
Structure	Preferential removal of amorphous carbon forms	Lower selectivity towards the carbon forms
Texture	Higher TSA at equivalent X and less damaged surface Development of mesoporosity besides microporosity Small micropore size distribution Preferential development of 1 nm micropores	Lower TSA and more damaged char surface Higher proportion of micropores Large micropore size distribution More laid micropores size
Minerals	Better retention of AAEM species Higher retention of Si and Al	Lower retention of AAEM species Lower retention of Si and Al

emissions.

4. Conclusions

The present work aimed at shedding light on the unfolding of the char gasification reaction under H_2O, CO_2 and their mixtures, leaning on a deep characterization of partially gasified chars obtained respectively at 0%, 20%, 50% and 70% of conversion. The char structure, texture, surface chemistry as well as the mineral contents were investigated along the three gasification reactions.

The results showed that H_2O and CO_2 gasification reactions have likely different pathways. The principal characteristics and marked differences between CO_2 and H_2O gasification reactions are summarized in Table 3:

The Raman spectra of the H_2O-chars show that H_2O reacts preferentially with D3 carbon form and probably induces ring condensation due to the presence of mobile H on the char surface. CO_2 do not show a clear selective reactivity towards a specific carbon form.

The char surface chemistry is different for the two reactions as CO_2 chars contains more emitting *CO* surface functions, while H_2O gasified chars are much more hydrogenated. H_2O appears to react preferably with ethers, phenols and anhydrides in the first stages of the reaction ($X < 20\%$). This observation can be correlated with the marked decrease of the I_{D3}/I_{D1} ratio observed in the Raman spectra of 20%-H_2O char compared to the Ref-char. Ethers, phenols and anhydrides are thought to contribute effectively to the D3 band intensity. Moreover, the marked increase of surface H atoms in the char, due to steam gasification, can be correlated to the decrease of the I_{D3}/I_{D1} ratio, as mobile H can induce ring condensation and thus increase the proportion of D1 carbon forms.

The textural properties of CO_2 and H_2O chars also differ. In deed, H_2O gasification leads to a higher internal char porosity than CO_2 at equivalent conversion levels, due to a more volumetric gasification reaction. H_2O gasification develops preferentially 1 nm micropores and creates mesoporosity along the conversion. The CO_2 gasification develops mainly micropores in the range of 10–20 Å with a larger bimodal pore distribution. The SEM observations as well as porosity measurements revealed that CO_2 gasification affects more the char surface than the particle core, which is probably related to a lower diffusivity of CO_2 compared to H_2O. Internal diffusional limitations are observed for the different atmospheres as very small micropores of 5–6 Å continue to be developed along the gasification reaction regardless of the atmosphere composition.

In mixed atmosphere gasification, the char SFG and Raman parameters are similar to those observed in the H_2O-chars. This has likely to do with a higher carbon removal via steam gasification. The CO_2 contribution to the gasification reaction is not negligible. The CO_2 TPD profile of Mix-chars appears as a blend of the CO_2 TPD profiles obtained for the single atmosphere chars, denoting the contribution of both reactions. In addition, it was found that the micropore size distributions of Mix-chars tend towards those of CO_2 chars exhibiting a bimodal distribution. The microporosity and small mesoporosity in the range of 20–50 Å is better developed in mixed atmosphere gasification than in single atmospheres.

As the bimodal pore size distribution was observed only for CO_2 and mixed atmosphere gasification, it is plausible that H_2O molecules facilitate the CO_2 molecules diffusion to the 11 Å pores. CO_2 molecules can then react on and induce their widening. In a similar way, for the 10 to 20 Å and 30 to 50 Å pores, it would be an enhanced CO_2 diffusivity inside this porosity in the presence of H_2O, which induce their much pronounced development by CO_2 gasification.

There may be consequently a competition between CO_2 and H_2O for the reaction on a part of the active surface, and simultaneously a synergy by an enhancement of the CO_2 internal diffusivity. Also, CO_2 was seen to enhance the departure of Si from the char matrix steam compared to the case of steam gasification. There may be also be synergistic effects in mixed atmosphere gasification due to the action of CO_2 on Si which is known to be an inhibitor of the steam gasification reaction.

As a general conclusion, CO_2 and H_2O reactions would follow different pathways. In mixed atmosphere gasification, these two molecules do not react independently since there are likely several competition and synergy interactions that lead to an apparent additive law of reactivity. Which can thought to be a separate active sites reactions mechanism, is rather a sum of a more complicated synergy and inhibition interactions. The additive law observed in the mixed atmosphere gasification would be only a fortuitous correct mathematical representation of the char reactivity in mixed atmospheres.

Acknowledgements

The authors want to thanks gratefully for their help: Joseph Dentzer for TPD-MS experiments, Habiba Nouali for textural analysis, Laure Michelin and Ludovic Josien for SEM and X-Ray fluorescence analysis. The authors also acknowledge the French National Research Agency for its financial support in the $RECO_2$ project. They also wish to express their appreciation to Bernard Auduc for his technical support.

References

[1] Bentsen Niclas Scott, Jack Michael W, Felby Claus, Thorsen Bo Jellesmark. Allocation of biomass resources for minimising energy system greenhouse gas emissions. Energy 2014;69:506–15.

[2] Kwak Tae Heon, Lee Seungmoon, Maken Sanjeev, Shin Ho Chul, Park Jin Won, Yoo Young Done. A study of gasification of municipal solid waste using a double inverse diffusion flame burner. Energy Fuels 2005;19(6):2268–72.

[3] Kwak Tae Heon, Maken Sanjeev, Lee Seungmoon, Park Jin W, Min Byoung ryul, Yoo Young Done. Environmental aspects of gasification of Korean municipal

solid waste in a pilot plant. Fuel 2006;85(14–15):2012–7.
[4] Kwak Tae-Heon, Lee Seungmoon, Park Jin-Won, Maken Sanjeev, Done Yoo Young, Lee Sang-Houck. Gasification of municipal solid waste in a pilot plant and its impact on environment. Korean J Chem Eng 2006;23:954–60.
[5] Imorb Karittha, Simasatitkul Lida, Arpornwichanop Amornchai. Techno-economic analysis of the biomass gasification and Fischer-Tropsch integrated process with off-gas recirculation. Energy 2016;94:483–96.
[6] Dupont Capucine, Jacob Sylvain, Ould Marrakchy Khalil, Hognon Céline, Grateau Maguelone, Labalette Françoise, et al. How inorganic elements of biomass influence char steam gasification kinetics. Energy 2016;109:430–5.
[7] Avila Claudio, Pang Cheng Heng, Wu Tao, Lester Ed. Morphology and reactivity characteristics of char biomass particles. Bioresour Technol April 2011;102(8):5237–43.
[8] Mermoud F, Salvador S, Vandesteene L, Golfier F. Influence of the pyrolysis heating rate on the steam gasification rate of large wood char particles. Fuel July 2006;85(10–11):1473–82.
[9] Senneca Osvalda. Kinetics of pyrolysis, combustion and gasification of three biomass fuels. Fuel Process Technol 2007;88(1):87–97.
[10] Gil María V, Riaza Juan, Álvarez Lucía, Pevida Covadonga, Rubiera Fernando. Biomass devolatilization at high temperature under N2 and CO2: char morphology and reactivity. Energy 2015;91:655–62.
[11] Bai Yonghui, Wang Yulong, Zhu Shenghua, Li Fan, Xie Kechang. Structural features and gasification reactivity of coal chars formed in Ar and CO2 atmospheres at elevated pressures. Energy 2014;74(C):464–70.
[12] Dupont Capucine, Nocquet Timothée, Augusto Da Costa José, Verne-Tournon Christèle. Kinetic modelling of steam gasification of various woody biomass chars: influence of inorganic elements. Bioresour Technol October 2011;102(20):9743–8.
[13] Fu Peng, Hu Song, Xiang Jun, Yi Weiming, Bai Xueyuan, Sun Lushi, et al. Evolution of char structure during steam gasification of the chars produced from rapid pyrolysis of rice husk. Bioresour Technol June 2012;114:691–7.
[14] Laine NR, Vastola FJ, Walker PL. The importance of active surface area in the carbon-oxygen reaction. J Phys Chem 1963;67:2030–4.
[15] Causton Peter, Brian McEnaney. Determination of active surface areas of coal chars using a temperature-programmed desorption technique. Fuel 1985;64:1447–51.
[16] Figueiredo JL, Pereira MFR, Freitas MMA, Orfao JJM. Modification of the surface chemistry of activated carbons. Fuel 1999;37:1379–89.
[17] Brender P, Gadiou R, Rietsch J-C, Fioux P, Dentzer J, Ponche A, et al. Characterization of carbon surface chemistry by combined temperature programmed desorption with in situ x-ray photoelectron spectrometry and temperature programmed desorption with mass spectrometry analysis. Anal Chem 2012;84:2147–53.
[18] Zhuang Qianlin, Kyotani Takashi, Tomita Akira. Dynamics of surface oxygen complexes during carbon gasification with oxygen. Energy & Fuels 1995;9(4):630–4.
[19] Klose W, Wolki M. On the intrinsic reaction rate of biomass char gasification with carbon dioxide and steam. Fuel May 2005;84(7–8):885–92.
[20] Asadullah Mohammad, Zhang Shu, Min Zhenhua, Yimsiri Piyachat, Li Chun-Zhu. Effects of biomass char structure on its gasification reactivity. Bioresour Technol June 2010;101(20):7935–43.
[21] Wornat Mary J, Hurt Robert H, Yang Nancy YC, Headley Thomas J. Structural and compositional transformations of biomass chars during combustion. Combust Flame January 1995;100(1–2):131–43.
[22] Tay Hui-Ling, Kajitani Shiro, Zhang Shu, Li Chun-Zhu. Effects of gasifying agent on the evolution of char structure during the gasification of Victorian brown coal. Fuel January 2013;103:22–8.
[23] Keown Daniel M, Hayashi Jun-Ichiro, Li Chun-Zhu. Drastic changes in biomass char structure and reactivity upon contact with steam. Fuel June 2008;87(7):1127–32.
[24] Li Tingting, Zhang Lei, Dong Li, Li Chun-Zhu. Effects of gasification atmosphere and temperature on char structural evolution during the gasification of Collie sub-bituminous coal. Fuel January 2014;117:1190–5.
[25] Henriksen Ulrik, Hindsgaul Claus, Qvale Bjø rn, Fjellerup Jan, Jensen Anker Degn. Investigation of the anisotropic behavior of wood char particles during gasification. Energy & Fuels September 2006;20(5):2233–8.
[26] Huang Yanqin, Yin Xiuli, Wu Chuangzhi, Wang Congwei, Xie Jianjun, Zhou Zhaoqiu, et al. Effects of metal catalysts on CO2 gasification reactivity of biomass char. Biotechnol Adv 2009;27(5):568–72.
[27] Hognon Céline, Dupont Capucine, Grateau Maguelone, Delrue Florian. Comparison of steam gasification reactivity of algal and lignocellulosic biomass: influence of inorganic elements. Bioresour Technol May 2014;164:347–53.
[28] Nzihou Ange, Stanmore Brian, Sharrock Patrick. A review of catalysts for the gasification of biomass char, with some reference to coal. Energy September 2013;58:305–17.
[29] Bouraoui Zeineb, Jeguirim Mejdi, Guizani Chamseddine, Limousy Lionel, Dupont Capucine, Gadiou Roger. Thermogravimetric study on the influence of structural, textural and chemical properties of biomass chars on CO_2 gasification reactivity. Energy 2015;88:703–10.
[30] Bouraoui Zeineb, Dupont Capucine, Jeguirim Mejdi, Limousy Lionel, Gadiou Roger. CO_2 gasification of woody biomass chars: the influence of K and Si on char reactivity. Comptes Rendus Chim 2016;19(4):457–65.
[31] Klinghoffer Naomi B, Castaldi Marco J, Nzihou Ange. Catalyst properties and catalytic performance of char from biomass gasification. Industrial Eng Chem Res October 2012;51(40):13113–22.
[32] Lopez-Gonzalez D, Fernandez-Lopez M, Valverde JL, Sanchez-Silva L. Gasification of lignocellulosic biomass char obtained from pyrolysis: kinetic and evolved gas analyses. Energy 2014;71:456–67.
[33] Lopez Gartzen, Alvarez Jon, Amutio Maider, Arregi Aitor, Bilbao Javier, Olazar Martin. Assessment of steam gasification kinetics of the char from lignocellulosic biomass in a conical spouted bed reactor. Energy 2016;107:493–501.
[34] Di Blasi Colomba. Combustion and gasification rates of lignocellulosic chars. Prog Energy Combust Sci April 2009;35(2):121–40.
[35] Pattanotai Teeranai, Watanabe Hirotatsu, Okazaki Ken. Experimental investigation of intraparticle secondary reactions of tar during wood pyrolysis. Fuel February 2013;104:468–75.
[36] Guizani C, Escudero Sanz FJ, Salvador S. Influence of temperature and particle size on the single and mixed atmosphere gasification of biomass char with H_2O and CO_2. Fuel Process Technol February 2015;134:175–88.
[37] Guizani C, Escudero Sanz FJ, Salvador S. The gasification reactivity of high-heating-rate chars in single and mixed atmospheres of H_2O and CO_2. Fuel June 2013;108:812–23.
[38] Jawhari T, Universitat De Barcelona, and De Investigacibn. Raman spectroscopic characterization of some commercially available carbon black materials. Carbon 1995;33(11):1561–5.
[39] Sadezky A, Muckenhuber H, Grothe H, Niessner R, Pöschl U. Raman microspectroscopy of soot and related carbonaceous materials: spectral analysis and structural information. Carbon July 2005;43(8):1731–42.
[40] Sheng C. Char structure characterised by Raman spectroscopy and its correlations with combustion reactivity. Fuel October 2007;86(15):2316–24.
[41] Chabalala VP, Wagner N, Potgieter-Vermaak S. Investigation into the evolution of char structure using Raman spectroscopy in conjunction with coal petrography; Part 1. Fuel Process Technol April 2011;92(4):750–6.
[42] Liu Xuhui, Zheng Ying, Liu Zhaohui, Ding Haoran, Huang Xiaohong, Zheng Chuguang. Study on the evolution of the char structure during hydrogasification process using Raman spectroscopy. Fuel October 2015;157:97–106.
[43] MATLAB. version 8.0 (R2012a). Natick, Massachusetts: The MathWorks Inc.; 2012.
[44] Haver Tom O. An introduction to signal processing in chemical analysis. 2009.
[45] Jagiello Jacek, Olivier James P. 2D-NLDFT adsorption models for carbon slit-shaped pores with surface energetical heterogeneity and geometrical corrugation. Carbon April 2013;55(2):70–80.
[46] Lowell S, Shields JE. Powder surface area and porosity. third edit Ed. Chapman and Hall; 1991.
[47] Marsh Harry, Rodriguez-reinoso Francisco. Activated carbon. Elsevier Science & Technology Books; 2006.
[48] Román S, González JF, González-García CM, Zamora F. Control of pore development during CO_2 and steam activation of olive stones. Fuel Process Technol August 2008;89(8):715–20.
[49] Klinghoffer Naomi. Utilization of char from biomass gasification in catalytic applications. PhD Thesis. New York, USA: Earth and Environmental Engineering Columbia University; 2013.
[50] Mitsuoka Keiichirou, Hayashi Shigeya, Amano Hiroshi, Kayahara Kenji, Sasaoaka Eiji, Uddin Md Azhar. Gasification of woody biomass char with CO2: the catalytic effects of K and Ca species on char gasification reactivity. Fuel Process Technol January 2011;92(1):26–31.
[51] Zhang Y, Ashizawa M, Kajitani S, Miura K. Proposal of a semi-empirical kinetic model to reconcile with gasification reactivity profiles of biomass chars. Fuel April 2008;87(4–5):475–81.
[52] Ghimbeu C, Gadiou R, Dentzer J, Vidal L, Vix-Guterl C. A TPD-MS study of the adsorption of ethanol/cyclohexane mixture on activated carbons. Adsorpt Sci Technol 2011;17:227–33.
[53] Karpinski Zbigniew, Szymanski Grzegorz S. The effect of the gradual thermal decomposition of surface oxygen species on the chemical and catalytic properties of oxidized activated carbon. carbon 2002;40:2627–39.
[54] Rietsch Jean-Christophe, Brender Patrice, Dentzer Joseph, Gadiou Roger, Vidal Loic, Vix-Guterl Cathie. Evidence of water chemisorption during graphite friction under moist conditions. Carbon 2013;55:90–7.